Wave propagation and scattering in reinforced concrete beams

Evelyne El Masri,[1,a)] Neil Ferguson,[1] and Timothy Waters[1]

Institute of Sound and Vibration Research, University of Southampton,

Southampton, SO17 1BJ, UK

Steel reinforcement bars (rebars) are vital to the strength of reinforced concrete (RC) structures, but can become damaged due to corrosion. Such damage is generally invisible and non-destructive testing methods are needed to assess their integrity. Guided wave methods are popular because they are capable of detecting damage using sensors placed remotely from the damage site, which is often unknown. This paper predicts free wave propagation in RC beams from which the concept of a guided wave based damage detection method emerges. The wave solutions are obtained using the wave finite element (WFE) framework where a short section of the beams cross section is modelled in conventional FE and periodic boundary conditions are subsequently applied. Reinforcement elements are used in the FE model of the cross section as a neat and efficient means of coupling the concrete to the rebars and imposing prestress. The results show that prestress, important for static behaviour, has a negligible effect on wave dispersion. An RC beam with a damaged section is modelled by coupling three waveguides, the centre waveguide being identical to the outer ones except for a thickness loss in one rebar. Only small differences in cut-on frequencies are observed between the damaged and undamaged sections. However, these small differences give rise to strong reflection of some waves at frequencies close to cut-on. Below cut-on, most incident power is transmitted but experiences wave mode conversion whereas above cut-on most power is transmitted to the same wave type. These observations form the basis for ongoing work to develop a damage detection technique premised on wave reflection near cut-on.

[a] E.El-Masri@soton.ac.uk

I. INTRODUCTION

Reliable, cost effective and more widespread nondestructive inspection of concrete structures is needed to reduce the occurrence of catastrophic failures. Vibration based methods have proved popular, particularly since they are potentially global, i.e. the effects of damage on vibration can be observed away from the damage site. A key limitation is the need to have either an accurate physical model of the undamaged structure or a reference set of measurements in the undamaged state. A comprehensive review by (Wang *et al.*, 2010) covered modal based approaches (natural frequency, mode shapes, modal strain energy and dynamic flexibility considerations) as well as non-physical models comprising Artificial Neural Networks (ANN) and time domain analysis of actual structural response measurements. Guided wave based methods, by contrast, do not typically require a reference state and are also independent of the often unknown boundary conditions. Modelling is, however, still essential to develop or tailor guided wave techniques for particular applications. Since RC beams are composite structures, analytical wave solutions do not exist and a numerical approach is needed. The Wave Finite Element method (WFE) is well suited to this scenario, whereby a short segment of the beam is initially modelled via FE. By applying periodicity, its free and forced wave propagation solutions can be obtained.

(Duhamel *et al.*, 2003) developed the WFE method for simple homogeneous one-dimensional waveguides including flexure of beams. This formulation involved the derivation of a Dynamic Stiffness Matrix for one segment of the waveguide that is then used in the derivation for the transfer function of the variables comprising the nodal displacements and forces across the segment, which in principle can be obtained from either an analytical model or a FE model realization. Subsequently, (Mace *et al.*, 2005) presented the flexural wavenumbers, energy and wave group velocity for structures comprising a beam, a simply supported plate strip and a viscoelastic laminate. Issues related to waves containing coupled displacements in more than one component direction were obtained as well as numerical ill conditioning issues were addressed. For each wave type, there is a corresponding displacement field or wave mode over the cross section. This can be used to discriminate between which free wave is propagating and its corresponding wavenumber at each frequency.

WFE is not restricted to structures composed of one material, as demonstrated by (Mencik and Ichchou, 2007) who formulated and solved wave propagation in guided elastodynamic structures filled with acoustic fluid. Free and forced frequency responses of the waveguide were presented, and comparisons between the proposed method and classical theories were formulated showing that this method is not limited to low frequencies. In a later application, (Waki *et al.*, 2009b)expressed free and forced vibrations and experimental validation for a tyre using WFE. Numerical issues were considered (Waki *et al.*, 2009a), and a robust numerical solution procedure was proposed which is used herein. It showed that it was possible when formulating the Dynamic Stiffness Matrix to use dynamic condensation, not Guyan Reduction, of the internal degrees of freedom for the modelled segment without introducing significant errors and so keeping the numerical size of the model determined by the number of degrees of freedom on the cross section of the segment.

In practice, continuous waveguides comprise only part of a complex structure and there is a need to model typically joints, attachments, interfaces, etc., which can result in scattering as well as being necessary for any finite structural frequency response calculation. For coupling of waveguides, a WFE-FE-WFE coupling approach was developed (Ichchou *et al.*, 2009). For a damage scenario, a diffusion matrix prediction model (DMM) was used to couple damaged and undamaged waveguides, where higher modes showed greater sensitivity to damage modelled as a through thickness notch in the section modelled by FE and coupled to the waveguides. In this application, when the wave modes across the section which propagate and incident onto the notch possess a characteristic length scale across the thickness similar to the notch depth then significant reflection can occur, whilst lower frequency wave modes pass across the notch section with small reflection. Therefore, the identification by reflected waves will be depth of notch and selected wave mode dependent. (Zhou and Ichchou, 2010b) subsequently extended the work to plates and expressed wave excitation and scattering using the WFE eigensolutions of the coupled structures as well as time domain predictions simulating scattered effects and subsequent spectrogram illustrating the significant reflection of incident A0 mode Lamb waves.

Another method, applicable for certain types of damage located in one section of a waveguide which still exhibits wave guide behaviour, is to model each waveguide via WFE. The approach is then to couple damaged and undamaged sections by coupling of the different waves, i.e. a WFE-WFE-WFE coupling model methodology. For instance, (Harland *et al.*, 2001) elegantly presented the reflection and transmission coefficients of wave modes comprising both displacement and force vector descriptions passing through two different beam waveguides. By considering the continuity and equilibrium equations at the junctions, the incident, reflected and transmitted waves can be related through WFE solutions in each waveguide. Finite ends and boundary conditions were also formulated, but no finite lengths were considered. The later study by (Lee *et al.*, 2007), which is applicable as background for this current paper, is the introduction of both the reflection and transmission calculation through a finite length connector separating two beams. An example considered the effect of a tapered length joining two rectangular cross section beams of different constant thickness producing results that are in good agreement to an exact solution. The wave propagation in the intermediate section involves both reflection and transmission matrices at the two interfaces in addition to propagation matrices for the wave amplitudes along its length. The concise formulation retains the physics with efficient and accurate computational solutions, involving wave conversion as well as power balance. This last papers focus was primarily introducing the methodology and wave conversion. It did not attempt to unravel the cut-on effect that could exist within the intermediate section, and what happens for waves already cut on in the first section that are then incident upon the intermediate section.

Mode conversion, providing subsequent reflection and transmission coefficients have also been used to localize damaged portions in a curved beam (Zhou and Ichchou, 2010a) and again this considered a notch type form of damage as considered by (Ichchou *et al.*, 2009). (Kharrat *et al.*, 2011)) also proposed the identification and sizing of defects in pipelines by WFE, using torsional guided waves with reflections proposed as a methodology to identify cracks represented by rectangular defects through the thickness and over a rectangular area and represented by a cylindrical section using an FE model. It again was a WFE-FE-WFE model, but the dynamic condensation for the FE modelled length was by Component Mode Synthesis (CMS) rather than condensation of the dynamic stiffness matrix, say, which would need to be performed at every frequency. Later work (Kharrat *et al.*, 2014)used WFE to extend the torsional wave model to construct a numerical database of reflection coefficients by varying the dimensions of the pipeline damage. This work also included experimental validation, showing the additional complication of attenuation in a complex pipework system. The experimental results for the reflection coefficient for the lowest order torsional mode on a single pipe are in good agreement with the WFE predictions over a range of frequencies. However, on a complex pipework system, with results only at three particular frequencies and no clear attempt to interpret what wave types were involved, it offers limited validation for a practical solution. (Renno and Mace, 2013) subsequently calculated the reflection and transmission coefficients for very general joints with multiple connected one-dimensional wave guide systems at one point using a hybrid FE/WFE approach, where again the joint was modelled via FE and a small portion of each waveguide is described via a corresponding WFE model. Comparison against analytical simplified models and full solid element FE models highlighted the need for a sufficiently accurately refined FE mesh using solid elements, which has been adopted herein.

A number of experimental studies in the literature use guided waves to detect damage in RC beams, e.g. (Amjad *et al.*, 2015). However, numerical characterization of free wave propagation in RC beams is limited. (Zima, 2019) contrasted the dispersion curves of a single rebar in vacuo with one embedded in a square concrete section, using the semi-analytical finite element (SAFE) method. (Yamakawa and Murakami, 1997) predicted the dispersion curves and wave mode shapes of a cylindrical concrete column with longitudinal rebars by applying Floquet boundary conditions to a unit cell modelled in finite elements. Tie bars were also included but found to be negligible. However, to the authors knowledge no wave based models have been developed that account for both the composite and preloaded nature of RC beams. The WFE methodology is directly applicable, but an accurate FE model of the section is first required. Modelling is complicated by pretension in the steel reinforcement bars (rebars) that prestress the concrete and by periodically placed vertical rebars (stirrups). In commercial software, such as ANSYS, concrete is typically modelled using solid (SOLID65) elements and the steel reinforcements represented via link (LINK8 or LINK180) elements (Badiger and Malipatil, 2014) (Jnaid and Aboutaha, 2015). Coupling is required between the solid and link elements to transfer prestress. (Li and Zhang, 2011) validated this approach through measured natural frequencies published in (Saiidi *et al.*, 1994). An alternative modelling approach has recently been implemented by (El Masri, 2018) using 3D discrete reinforcing elements, REINF264 (ANSYS, 2013). This obviates the need for coupling elements, reduces the number of degrees of freedom (DOFs) and produces comparable results to those published by (Li and Zhang, 2011).

In this paper, free wave propagation is studied in uniform and non-uniform prestressed reinforced concrete (RC) beams using the WFE method. Sec. (II) provides a brief synopsis of the WFE method and describes its implementation for RC beams. Dispersion curves are presented, which are subsequently validated experimentally in Sec. (III). Sec. (IV) describes how three waveguides obtained by WFE can be coupled to model a piecewise uniform waveguide where the centre section may, for example, represent damage. It is verified that, for the case when loss of thickness is applied to one rebar, the reflection coefficients are identical to those obtained by the established approach of coupling in an FE model of the discontinuity. However, the former approach is more conducive to physical interpretation of the wave behaviour. In Sec. (V), the model is used to study wave scattering in the case of an RC beam with a local loss of thickness in one rebar. Some wave modes exhibit strong reflection in a narrow frequency band where a wave starts to propagate in the undamaged section but is still evanescent in the damaged section. Conclusions are drawn in Sec. (VI) which are related to ongoing research activities to develop a damage detection method for RC beams based upon this behaviour.

II. WFE MODELLING OF RC BEAMS

The WFE method is an established method for computing free wave propagation in uniform or periodic waveguides which can be represented by a chain of identical cells, as shown in Fig. 19. An FE model is created of one cell such that the nodes and their associated DOFs are ordered identically on the left and right sides. In the case of a uniform waveguide the cell is typically just one element long. Nodal forces and displacements on one side of the cell are related to those on the other side by a transfer matrix that is a function of frequency and the global FE mass and stiffness matrices. The propagation of a wave of wavenumber k along a cell invokes a phase shift of $k\Delta$ between the left and right nodal forces and displacements. An eigenvalue problem is obtained for each frequency, where the eigenvalues relate to wavenumber solutions of right and left propagating waves and the eigenvectors are the associated force and displacement wave mode shapes. An outline of the method is given in an appendix, and the interested reader is referred to (Duhamel *et al.*, 2006) for further details.

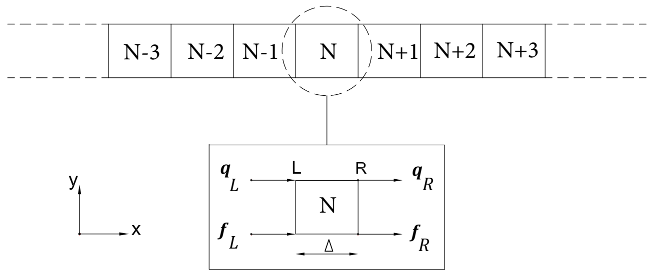

FIG. 1. Structure with periodic elements: the cell N with segment length Δ is shown with the vectors for the internal forces and displacements.

The evolution with frequency of individual waves can be tracked, and hence dispersion curves drawn, by pairing similar wave mode shapes between one frequency and the next. In this paper similarity is quantified using the Wave Assurance Criterion (Houillon *et al.*, 2005):

$$\mathrm{WAC}(u, v) = \frac{({}^t u.\bar{v})({}^t v.\bar{u})}{({}^t u.\bar{u})^2({}^t v.\bar{v})^2}. \tag{1}$$

where two complex eigenvectors u and v are associated with two distinct eigenvalues, and t is the transpose formation.If the WAC number is close to the unity, then the two eigenvectors u and v at two consecutive steps correspond to the same eigenvalue.

The WFE methodology is used here to compute the dispersion curves and associated wave mode shapes of a uniform deep RC beam, as shown in Fig. 2, with and without prestress. The reinforced concrete section is modelled using 16 SOLID65 elements, as shown in Fig. 3(a), using the properties listed in Table I. The horizontal rebars are modelled via the embedded approach using REINF264 elements. The vertical stirrups are neglected. The length Δ of the segment is set equal to 0.01 m, the total number of DOFs n, is 150, and a hysteretic damping value η of 0.004 is chosen. A second damaged model was created in which the bottom right rebar was reduced in thickness by 36%, as shown in Fig. 3(b).

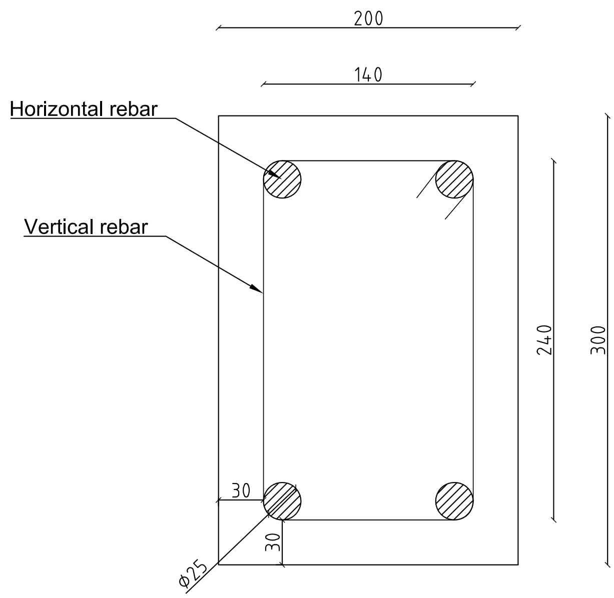

FIG. 2. Cross section details of the RC beam reinforcement.

TABLE I. Material properties for concrete and steel.

Material properties	Concrete	Steel
Young Modulus E (Pa)	40×10^9	200×10^9
Poisson ratio υ	0.18	0.3
Density ρ (kg/m^3)	2400	7850

Prestress is modelled via an initial strain in the rebars in a preliminary load stage. The initial static strain value is then calculated based on the steel reinforcement material properties and the prestress force applied. It is assumed that the tensile prestress force of the

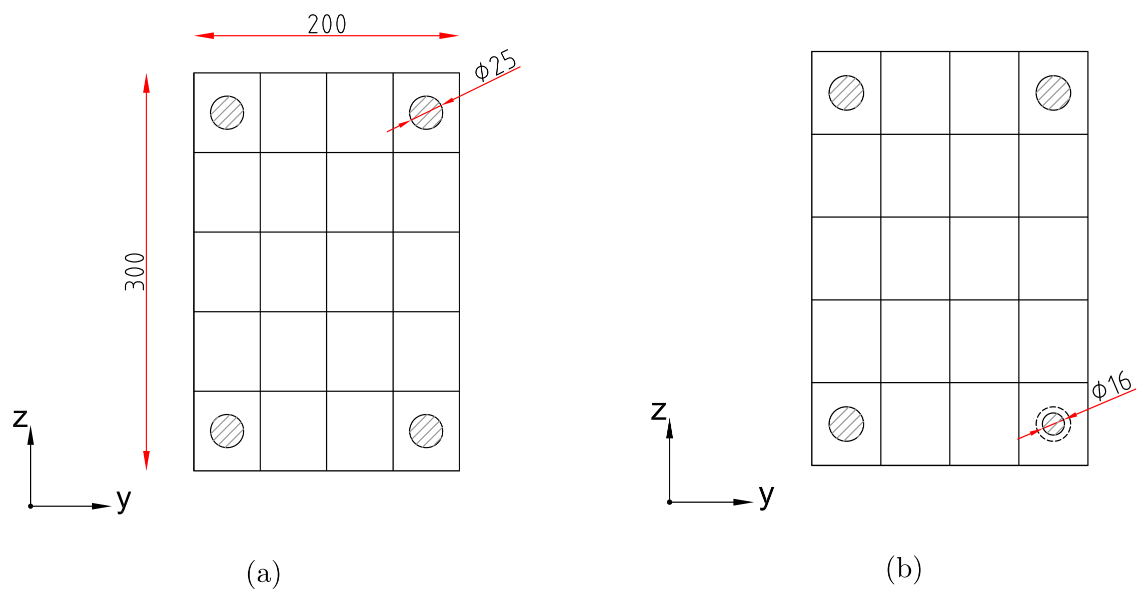

FIG. 3. FE mesh of RC sections (a) undamaged and (b) damaged with a rebar diameter reduction of 36%. Dimensions in mm.

steel reinforcement is equal to 70 percent of its ultimate tensile strength (0.4×10^9 Pa). This force is used to prestress both the damaged and undamaged rebars. Thus the stress value used to calculate the initial strain for the damaged rebar is higher than that for the undamaged one, since the cross sectional area is smaller for the same amount of prestress force. Subsequently, $\varepsilon_1 = 0.0014$ and $\varepsilon_2 = 0.0036$ are the initial longitudinal strain values for the original and reduced diameter rebars respectively.

The dispersion curves for an undamaged RC beam with and without prestress are shown in Fig. 4. The effect of prestress is to shift the curves slightly to the right owing to a small increase in stiffness. Hereafter, prestress is omitted from the model.

The dispersion curves for the RC beam with and without the rebar loss of thickness are shown in Fig. 5 (fundamental modes 1 to 4) and Fig. 6 (cut-on waves, denoted here by their cut-on frequency prefixed by E). Only slight changes are apparent between the behaviour

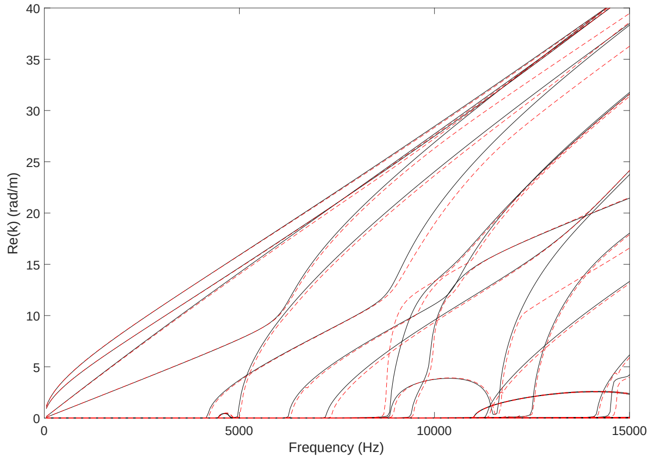

FIG. 4. Dispersion curves for the real part of the wavenumbers. RC section (—), prestress RC section (– – –).

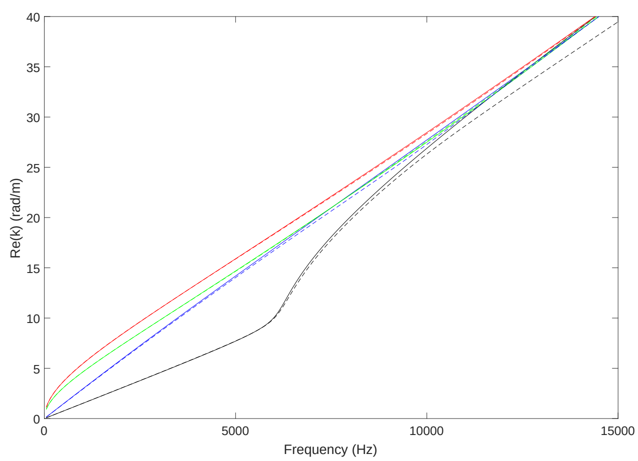

FIG. 5. Dispersion curves for the real part of the wavenumbers for propagating wave modes in an RC beam. Original RC section (—), reduced rebar section (- - -): mode 1 axial (-), mode 2 torsional (–), mode 3 bending (–) and mode 4 transverse bending (–).

of damaged and undamaged RC beams, from which it is concluded that dispersion curve measurement is not a suitable basis for damage detection. The cut-on frequencies are shifted

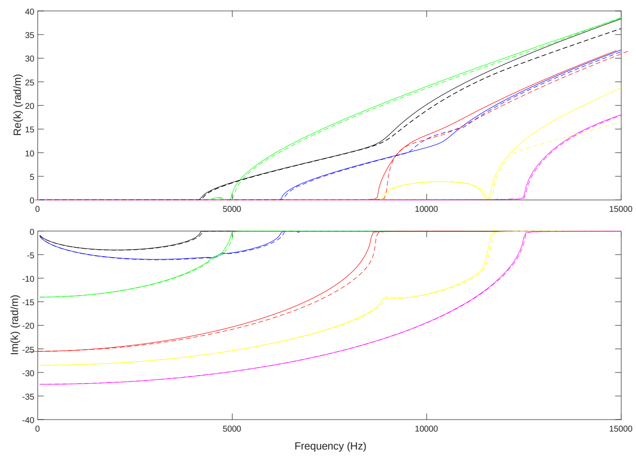

FIG. 6. Dispersion curves for the evanescent wave modes of an RC beam. Undamaged section (—), damaged section (- - -): E4200 (-), E5000 (—), E6300 (—), E8700 (—), E11700 (—), E12500 (—). E denotes an evanescent wave with its associated cut-on frequency in Hz.

slightly to the right due to reduction of rebar thickness, the loss of steel mass being more influential since the overall stiffness is dominated by the concrete.

In-plane modal displacements corresponding to the fundamental modes at 1kHz are shown in Fig. 7, and evanescent waves at their respective cut-on frequencies are shown in In-plane modal displacements corresponding to the fundamental modes at 1kHz are shown in Fig. 8. Mode 1 is associated with axial motion, mode 2 with torsional displacements around the x-axis, and modes 3 and 4 with bending in the vertical and transverse directions. Initially evanescent modes E5000, E8700, E11700 and E 12500 feature deformation in the plane of the cross section whereas modes E4200 and E6300 are predominantly axial owing to the small value of Poisson ratio used for concrete.

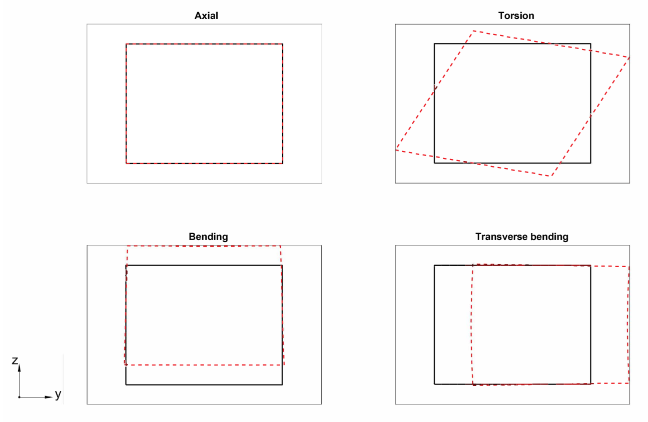

FIG. 7. Nodal displacements in the plane of the cross section (Y and Z directions) for selected propagating wave modes in an undamaged RC section. Undeformed section (—), deformed section (− − −) at 1000 Hz.

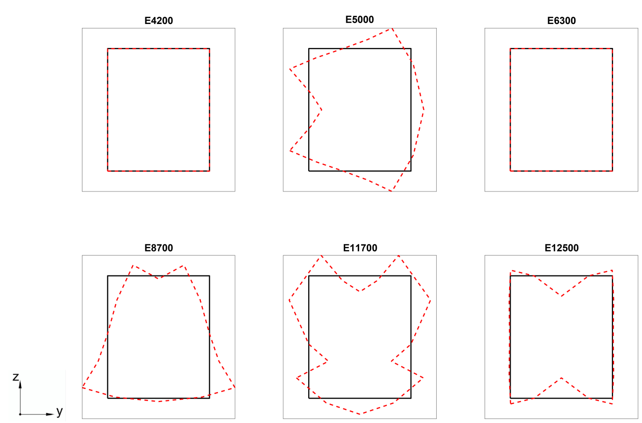

FIG. 8. Nodal displacements in the plane of the cross section (Y and Z directions) for selected evanescent wave modes in an undamaged RC section. Undeformed section (—), deformed section (− − −). E denotes an evanescent with its associated cut-on frequency.

III. EXPERIMENTAL VALIDATION OF WAVES IN RC BEAMS

The experimental validation comprised testing three RC beams of dimensions 0.2m×0.3m×2m; one had intact reinforcements and the other two had a 200 mm long section where the diameter of one rebar had been reduced. Grade 60 steel reinforcements were used for each beam, which were separated into horizontal and vertical (stirrup) rebars as illustrated in Fig. 8. The undamaged horizontal rebars are uniform and 25 mm in diameter whilst the damaged ones show a reduction to 16 mm and 10 mm respectively, as shown in Fig. 9. The horizontal and vertical reinforcements were tied together using steel fibres.

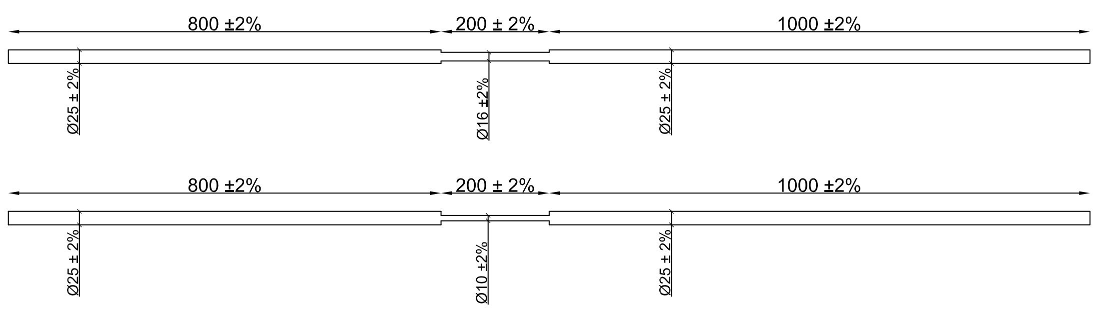

FIG. 9. Details of the damaged (reduced rebar) steel reinforcements.

After forming and curing, cylindrical concrete samples were crushed to identify the concrete's compressive strength f_c'. The average strength was found to be 70 MPa. One can relate the concrete's compressive strength f_c' to its Young's Modulus E_c in MPa using (ACI, 1995)

$$E_c = 4700\sqrt{f_c'}. \tag{2}$$

The associated Young's Modulus of concrete at 28 days was found to be approximately 38.9 GPa.

Roller boundary conditions were realized at both ends of the RC beams, see Fig. 10. An instrumented force hammer (PCB 086C03) was used to excite the structure in the vertical plane of symmetry, at a point 0.3 m from the left hand end. A hard tip was chosen to maximize bandwidth of the input. A roving miniature ICP accelerometer (PCB 352C22) was used to measure the vertical transient response at 20 positions from 0.5 to 1.5 m (including the damaged region), and transfer accelerances were computed.

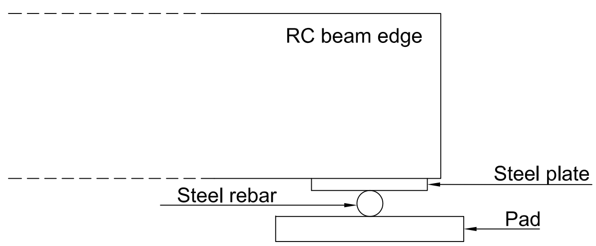

FIG. 10. RC beam roller boundary details.

Assuming a single wave type to be dominant at any one frequency, then an approximately harmonic spatial variation in response is expected along the beam. Its correlation to a sinusoid of trial wavenumber k_t can be estimated by (Ferguson *et al.*, 2002),

$$\hat{W}(k_x, \omega) \approx \sum_{i=1}^{N} w(x_i, \omega) e^{-ik_x x_i}. \tag{3}$$

where $\hat{W}(k_{tx}, \omega)$) is the frequency response at frequency omega and position x_i. The value of trial wavenumber that gives the highest correlation coefficient is selected as a point in the wavenumber-frequency plane. The trial wavenumber was selected within the range of 0 to 50 rad/m with a step size of 0.2 rad/m.

Fig. 11 shows the dispersion curves estimated from measurements of both the undamaged and damaged beams. The inclusion of some transducer measurements in the damaged region of two of the beams has not adversely affected estimation of the dispersion curves. The correlation technique successfully extracts multiple branches which are in close agreement with WFE predictions, also shown. Axial, torsional, transverse bending, and some higher order modes are not observed given the positions and orientations of the input and response sensors.

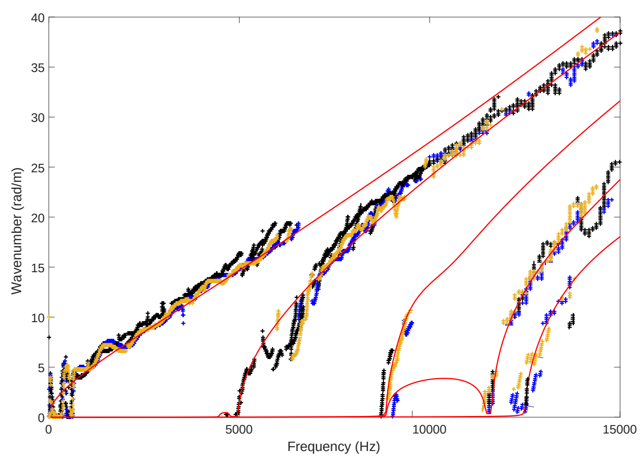

FIG. 11. Predicted and estimated wavenumbers for the damaged and undamaged RC beams after 28 days . WFE predicted wavenumbers (−), undamaged original beam (+), reduced rebar with 36% diameter reduction (+) and 60% diameter reduction (+).

Accelerance measurements were also taken at five points across the top and five points down one side of the cross section of the undamaged RC beam at a single position along its length. The operating deflection shapes at the cut-on frequencies of three of the wave modes are illustrated in Fig. 12 and Fig. 13. Good agreement is seen between these and the predicted wave mode shapes shown in Fig. 8.

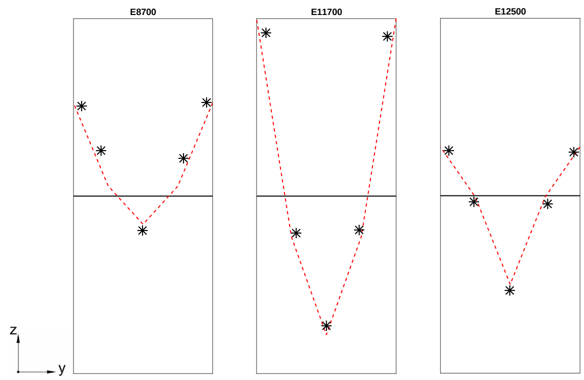

FIG. 12. Nodal displacements on the top surface in the Z direction for selected evanescent wave modes at cut-on frequencies of undamaged RC beam. Undeformed section (—), WFE deformed section (− − −), experimental deformed section (∗). E denotes evanescent with its associated cut-on frequency.

IV. COUPLING OF WAVEGUIDES

The WFE method has been used previously to model semi-infinite waveguides joined by a discontinuity which is modelled in FE, referred to here as the WFE-FE-WFE method. The system is then coupled using continuity and equilibrium conditions (Ichchou *et al.*, 2009). The advantage of this approach is that discontinuities of arbitrary geometry can be accommodated. However, when the discontinuity can itself be approximately represented as a uniform waveguide then it is more computationally efficient and physically insightful to couple three waveguides which are all similarly modelled in WFE, denoted WFE-WFE-WFE here, as shown in Fig. 14. Analysis for this original approach is derived as follows.

In Fig. 14, waveguides 1 and 3 represent identical beams whereas waveguide 2 is of finite length and different materially or geometrically due to damage, for example. Each is

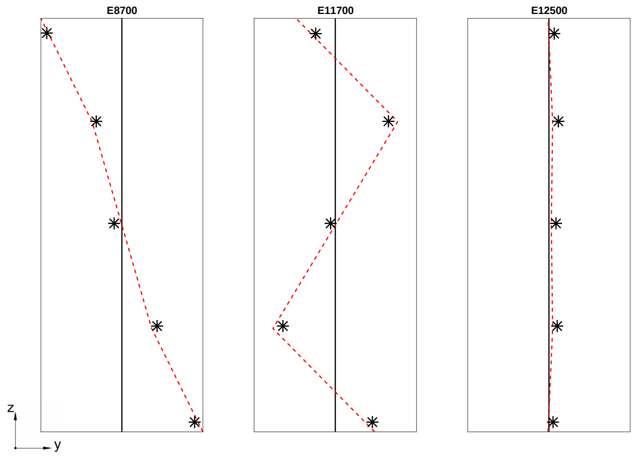

FIG. 13. Nodal displacements in the Y direction of selected evanescent wave modes at cut-on frequencies on the side surface of undamaged RC beam. Undeformed section (—), WFE deformed section (− − −), experimental deformed section ($*$). E denotes evanescent with its associated cut-on frequency.

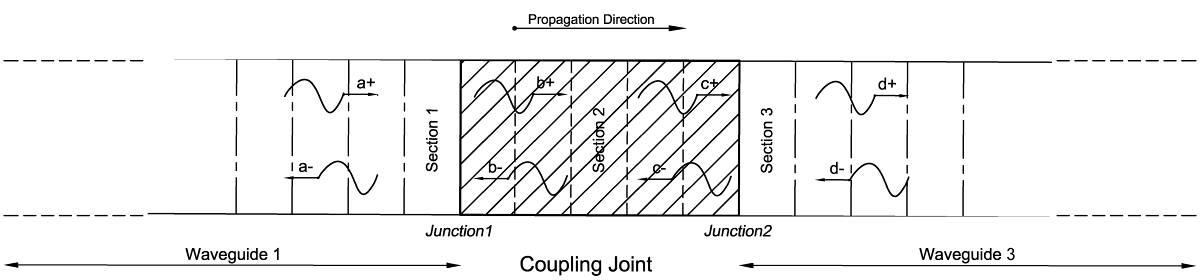

FIG. 14. The interface between wave finite elements waveguides: Sections 1, 2 and 3.

modelled in WFE using a segment of length Δ_i). In order to obtain the scattering matrix due to the finite section, one should first obtain the scattering matrices for the two junctions.

At junction 1, define $\boldsymbol{a}^-$ and $\boldsymbol{b}^+$ as the amplitudes of the wave modes scattered by the coupling element interface. $\boldsymbol{a}^+$ and $\boldsymbol{b}^-$ are the amplitudes of the wave modes incident onto the coupling element interface. Furthermore, $\boldsymbol{\Phi}^+$ and $\boldsymbol{\Phi}^-$ are matrices of right eigenvectors, where each wavemode is divided into displacement $\boldsymbol{q}$ and force $\boldsymbol{f}$ sub-vectors. The displacements and forces in waveguides 1 and 2 are given by

$$\boldsymbol{q}_1 = \boldsymbol{\Phi}^+_{q_1}\boldsymbol{a}^+ + \boldsymbol{\Phi}^-_{q_1}\boldsymbol{a}^- \;\; ; \;\; \boldsymbol{f}_1 = \boldsymbol{\Phi}^+_{f_1}\boldsymbol{a}^+ + \boldsymbol{\Phi}^-_{f_1}\boldsymbol{a}^-. \tag{4}$$

$$\boldsymbol{q}_2 = \boldsymbol{\Phi}^+_{q_2}\boldsymbol{b}^+ + \boldsymbol{\Phi}^-_{q_2}\boldsymbol{b}^- \;\; ; \;\; \boldsymbol{f}_2 = \boldsymbol{\Phi}^+_{f_2}\boldsymbol{b}^+ + \boldsymbol{\Phi}^-_{f_2}\boldsymbol{b}^-. \tag{5}$$

where $\boldsymbol{\Phi}^+$ and $\boldsymbol{\Phi}^-$ are matrices of right and left propagating waves, and are partitioned into displacements and forces as eigenvectors pertaining to Eq. (A.8).

Continuity of displacements and equilibrium of forces at junction 1 can then be expressed by

$$\boldsymbol{q}_1 = \boldsymbol{q}_2 \;\; ; \;\; \boldsymbol{f}_1 = \boldsymbol{f}_2. \tag{6}$$

The amplitudes of incident and scattered waves can be related by substituting Eq. (4) and Eq. (5) into Eq. (6) to give

$$\begin{bmatrix} -\boldsymbol{\Phi}^-_{q_1} & \boldsymbol{\Phi}^+_{q_2} \\ -\boldsymbol{\Phi}^-_{f_1} & \boldsymbol{\Phi}^+_{f_2} \end{bmatrix} \begin{Bmatrix} \boldsymbol{a}^- \\ \boldsymbol{b}^+ \end{Bmatrix} = \begin{bmatrix} \boldsymbol{\Phi}^+_{q_1} & -\boldsymbol{\Phi}^-_{q_2} \\ \boldsymbol{\Phi}^+_{f_1} & -\boldsymbol{\Phi}^-_{f_2} \end{bmatrix} \begin{Bmatrix} \boldsymbol{a}^+ \\ \boldsymbol{b}^- \end{Bmatrix}. \tag{7}$$

The scattering matrix $\mathbf{S}_1$ at Junction 1 is defined as

$$\begin{Bmatrix} \boldsymbol{a}^- \\ \boldsymbol{b}^+ \end{Bmatrix} = \mathbf{S}_1 \begin{Bmatrix} \boldsymbol{a}^+ \\ \boldsymbol{b}^- \end{Bmatrix}. \tag{8}$$

Then,

$$\mathbf{S}_1 = \begin{bmatrix} -\boldsymbol{\Phi}^-_{q_1} & \boldsymbol{\Phi}^+_{q_2} \\ -\boldsymbol{\Phi}^-_{f_1} & \boldsymbol{\Phi}^+_{f_2} \end{bmatrix}^{-1} \begin{bmatrix} \boldsymbol{\Phi}^+_{q_1} & -\boldsymbol{\Phi}^-_{q_2} \\ \boldsymbol{\Phi}^+_{f_1} & -\boldsymbol{\Phi}^-_{f_2} \end{bmatrix}. \tag{9}$$

The scattering matrix $\mathbf{S}_1$ is a block matrix where the diagonal matrices comprise the reflection coefficients, and the off-diagonal matrices contain the transmission coefficients. Subsequently, the scattering matrix $\mathbf{S}_1$ is defined as

$$\mathbf{S}_1 = \begin{bmatrix} \mathbf{R}_{12} & \mathbf{TM}_{21} \\ \mathbf{TM}_{12} & \mathbf{R}_{21} \end{bmatrix}. \tag{10}$$

where $\mathbf{R}$ and $\mathbf{TM}$ are the reflection and transmission matrices at the junction. In addition, the subscripts 1 and 2 are used to indicate the reflection and transmission matrices when the wave is incident from waveguide 1 to 2 respectively. Using the same procedure and definitions, the scattering matrix $\mathbf{S}_2$ at Junction 2 is defined as

$$\mathbf{S}_2 = \begin{bmatrix} -\boldsymbol{\Phi}^-_{\boldsymbol{q}_2} & \boldsymbol{\Phi}^+_{\boldsymbol{q}_3} \\ -\boldsymbol{\Phi}^-_{\boldsymbol{f}_2} & \boldsymbol{\Phi}^+_{\boldsymbol{f}_3} \end{bmatrix}^{-1} \begin{bmatrix} \boldsymbol{\Phi}^+_{\boldsymbol{q}_2} & -\boldsymbol{\Phi}^-_{\boldsymbol{q}_3} \\ \boldsymbol{\Phi}^+_{\boldsymbol{f}_2} & -\boldsymbol{\Phi}^-_{\boldsymbol{f}_3} \end{bmatrix}. \tag{11}$$

with

$$\mathbf{S}_2 = \begin{bmatrix} \mathbf{R}_{23} & \mathbf{TM}_{32} \\ \mathbf{TM}_{23} & \mathbf{R}_{32} \end{bmatrix}. \tag{12}$$

After solving for the scattering matrices at each junction, the total scattering matrix due to the finite length coupling element is derived based on the reflection and transmission matrices of each junction and the coupling joint propagation matrix. It is assumed that $\boldsymbol{d}^-$, the incident waves from the right, is zero since it is a semi-infinite beam (the Sommerfeld radiation condition). Using Eq. (8), and Eq. (10)

$$\boldsymbol{a}^- = \mathbf{R}_{12}\boldsymbol{a}^+ + \mathbf{TM}_{21}\boldsymbol{b}^-. \tag{13}$$

Let $\mathbf{F}$ be the propagation matrix between the two edges of the coupling element of length h, and let k_i be the wavenumbers associated with it. Then,

$$\mathbf{F} = \begin{bmatrix} e^{-i(k_1^+)h} & \cdots & 0 \\ \vdots & \ddots & \vdots \\ 0 & \cdots & e^{-i(k_n^+)h} \end{bmatrix}. \tag{14}$$

Hence $\mathbf{b}^-$ and $\mathbf{b}^+$ are related as follows,

$$\boldsymbol{b}^- = \mathbf{F}\mathbf{R}_{23}\mathbf{F}\boldsymbol{b}^+. \tag{15}$$

with

$$\boldsymbol{b}^+ = \mathbf{TM}_{12}\boldsymbol{a}^+ + \mathbf{R}_{21}\boldsymbol{b}^-. \tag{16}$$

Then,

$$\boldsymbol{b}^- = \mathbf{F}\mathbf{R}_{23}\mathbf{F}[\mathbf{I} - \mathbf{R}_{21}\mathbf{F}\mathbf{R}_{23}\mathbf{F}]\mathbf{TM}_{12}\boldsymbol{a}^+. \tag{17}$$

Substituting Eq. (17) into Eq. (13) gives

$$\boldsymbol{a}^- = \mathbf{R}_T\boldsymbol{a}^+ \;\; ; \;\; \mathbf{R}_T = \mathbf{R}_{12} + \mathbf{TM}_{21}\mathbf{F}\mathbf{R}_{23}\mathbf{F}[\mathbf{I} - \mathbf{R}_{21}\mathbf{F}\mathbf{R}_{23}\mathbf{F}]\mathbf{TM}_{12}. \tag{18}$$

Subsequently, $\mathbf{R}_T$ is the net reflection matrix due to the full finite length of the coupling element. Using Eq. (12), the net transmission matrix $\mathbf{TM}_T$ can be similarly derived as

$$\boldsymbol{d}^+ = \mathbf{TM}_T\boldsymbol{a}^+ \;\; ; \;\; \mathbf{TM}_T = \mathbf{TM}_{23}\mathbf{F}[\mathbf{I} - \mathbf{R}_{21}\mathbf{F}\mathbf{R}_{23}\mathbf{F}]\mathbf{TM}_{12}\boldsymbol{a}^+. \tag{19}$$

Subsequently, the full scattering matrix of the coupling element is given by

$$\begin{Bmatrix} \boldsymbol{a}^- \\ \boldsymbol{d}^+ \end{Bmatrix} = \begin{bmatrix} \mathbf{R}_T \\ \mathbf{TM}_T \end{bmatrix} \begin{Bmatrix} \boldsymbol{a}^+ \end{Bmatrix}. \tag{20}$$

The WFE-WFE-WFE approach is first verified against the WFE-FE-WFE method for the case of an RC beam with 36% loss of thickness in one rebar considered previously in Sec. (II) and Sec. (III). Fig. 15 shows the magnitudes of all diagonal elements of the reflection coefficient matrix, i.e. pertaining to no wave mode conversion.

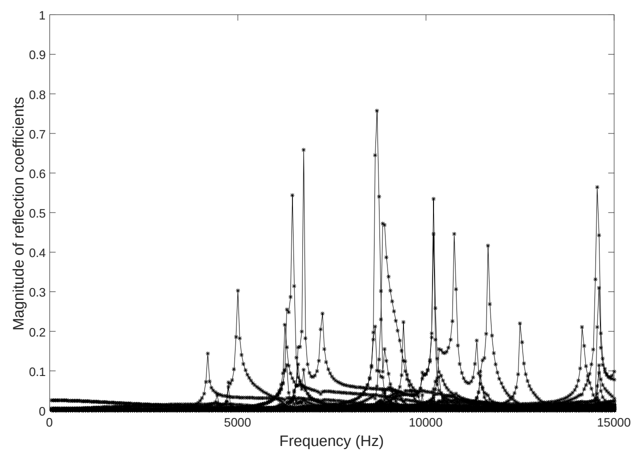

FIG. 15. Magnitude of the reflection coefficients due to simulated damage in RC beam. 36% reduction of one of steel diameter over a length $h = 0.2$ m and element size of 0.01 m. WFE-FE-WFE approach (—), WFE-WFE-WFE approach ($*$).

Whilst the two methods give apparently identical results, different numerical issues may arise.

1. The WFE-FE-WFE approach requires dynamic condensation to eliminate internal nodes which can cause ill-conditioning errors as the number of degrees of freedom increases, although conditioning can be improved by exploiting orthogonality of the left and right eigenvectors (Renno and Mace, 2013). The WFE-WFE-WFE approach, by contrast, does not require condensation since there are no internal nodes for a cell that is one element in length.

2. The WFE-WFE-WFE approach requires selection of an appropriate segment length, which is not to be too small with respect to the shortest wavelength to avoid round-off errors, nor too large to reduce discretization errors.

The WFE-WFE-WFE approach is chosen here for convenience since the length of the intermediate section can be changed without remodelling it in FE analysis.

V. WAVE SCATTERING DUE TO SIMULATED DAMAGE IN RC BEAMS

In this section, wave scattering is considered in detail for an RC beam with loss of rebar thickness over a finite length. Both undamaged and damaged RC sections are modelled and coupled together as described in Sec. (III) and Sec. (IV). Two lengths of damaged section were considered, $h = 0.05$ m and 0.2 m, for rebar diameter reductions of 36% and 60%. Fig. 16(a) to (d) show the magnitude of the reflection coefficients for all four damage permutations. The multiple curves in each subfigure correspond to different waves that cut-on below 15kHz. For each wave, reflection is negligible except at a narrow frequency band around cut-on. This is due to the wave propagating in the undamaged section but being evanescent in the damaged section. The peak reflection coefficient is wave dependent and is as high as 0.5 for the least damaged case Fig. 16(a) and 0.9 for the most severe damage in Fig. 16(d).

Of the waves whose mode shapes are shown in Fig. 8, E5000, E8700 and E11700 feature the most cross sectional deformation and exhibit prominent peaks in reflection coefficients in Fig. 16(d). By comparison, Fig. 17 shows the magnitude of the reflection coefficients for the fundamental wave modes (axial, torsional, bending and transverse bending) for the most

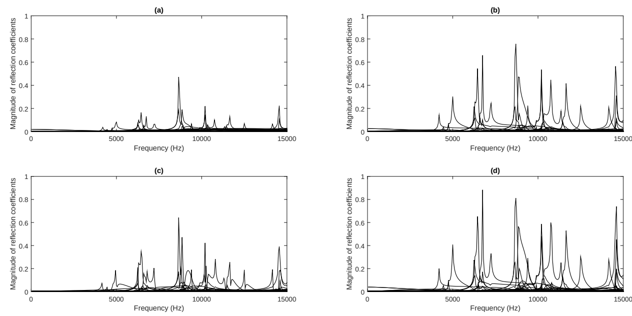

FIG. 16. Magnitude of the reflection coefficients due to simulated damage in RC beam.(a),(b) 36% reduction of one of steel diameter over a length $h = 0.05$ and 0.2 m,respectively; (c),(d) 60% reduction of one of steel diameter over a length $h = 0.05$ and 0.2m, respectively.

severe damage case. The coefficients are more than an order of magnitude smaller for these waves since they do not exhibit cut-on.

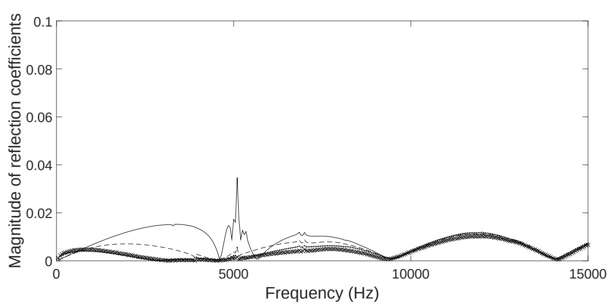

FIG. 17. Magnitude of the reflection coefficients of fundamental wave modes in an RC section with a 60% single rebar diameter reduction damage over a length h =0.2 m. Axial (—), torsional (- - -), bending(. . .), bending transversal (x.).

Power flow calculations were performed, using the analysis reported in (Mitrou *et al.*, 2017), to ascertain the extent of wave mode conversion both at and either side of wave cut-on.

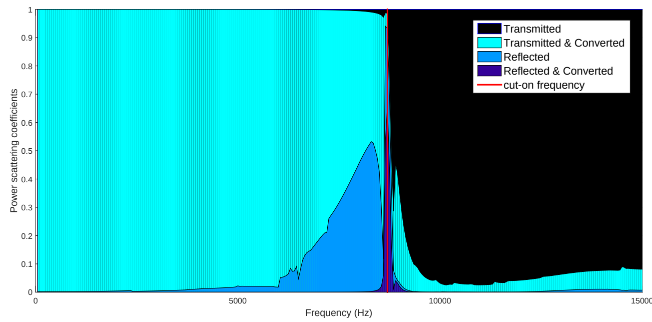

FIG. 18. Area plot of power scattering coefficients for incident wave E8700.

Fig. 18 shows an area plot of the power scattering coefficients for an incident wave E8700, which is typical of other wave types that cut-on in the frequency range of interest. The powers are partitioned as follows:

– Transmitted power to E8700

– Transmitted power converted to all other modes

– Reflected power to E8700

– Reflected power converted to all other modes

At cut-on, about 60% of the power is reflected into the same wave mode, which is potentially useful for damage detection purposes. Below cut-on, most power is transmitted but converted to other wave modes. Above cut-on, power is predominantly transmitted into the same wave mode, i.e. the rebar damage is reasonably transparent.

VI. CONCLUSIONS

Guided waves have proven an effective basis for long range detection of defects in many types of structure. This paper is motivated specifically by corrosion detection of rebars in reinforced concrete beams using guided waves, for which a physical understanding of the waves borne by the composite structure is essential. The WFE method has been used to model free wave propagation in RC beams. The FE model of the cross section, which forms the basis of the WFE model, uses embedded reinforcing elements to couple the concrete and rebar elements by which prestress is transferred to the concrete. Dispersion curves and associated wave mode shapes have been computed and successfully validated through measurements on laboratory samples. The effect of prestress on wave dispersion is shown to be negligible.

A new formulation has been presented to couple three waveguides which have been modelled using WFE. The analysis was used to predict wave scattering due to a uniform but damaged section of beam joined at both ends by undamaged sections. Damage was simulated by a loss of thickness of one of the rebars. It was found that, whilst the dispersion curves of the damaged and undamaged lengths are very similar, the slight difference in cut-on frequencies give rise to significant reflection of some waves which is potentially useful for the purpose of damage detection. The reflection occurs when a wave is able to propagate in the undamaged section of the beam but is evanescent in the damaged section, or vice versa. Powerflow analysis reveals that wave mode conversion is significant only below wave cut-on. Above cut-on, waves are unimpeded by the damage scenarios considered.

Ongoing work is focusing on methods to quantify wave reflection in the vicinity of wave cut-on but without any prior knowledge of the cut-on frequencies. An important practical constraint is that both actuation and sensing of guided waves must be performed on the accessible surfaces of the beam, .e.g. by means of an instrumented force hammer and accelerometer(s). An understanding of the wave mode shapes is useful for informing the placement and orientation of transducers, as well as identifying the particular wave modes of interest.

ACKNOWLEDGMENTS

The authors acknowledge the funding provided by the University of Southampton, the Lebanese Association of Scientific Research (LASeR) and Azm & Saade Association.

APPENDIX: DERIVATION OF WAVE FINITE ELEMENT METHOD

Consider a short length Δ of a uniform waveguide as shown schematically in Fig. 19 which is modelled using FE analysis such that the nodes and their associated DOFs are ordered identically on the left and right sides.

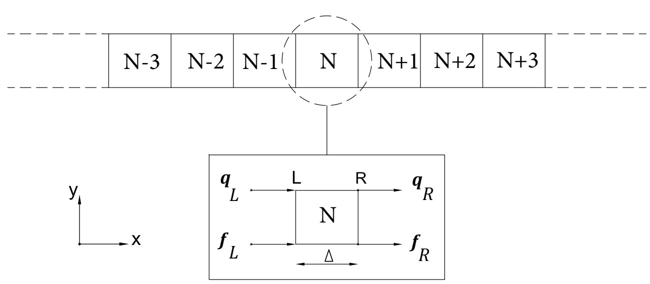

FIG. 19. Structure with periodic elements: the cell N with segment length Δ is shown with the vectors for the internal forces and displacements.

Time harmonic motion $e^{i\omega t}$ is implicit throughout this paper and suppressed for brevity. The nodal displacements q and forces f are related as follows (Duhamel *et al.*, 2006)

$$\mathbf{D}\boldsymbol{q} = \boldsymbol{f}. \tag{A.1}$$

Where the dynamic stiffness matrix

$$\mathbf{D} = \mathbf{K} - \omega^2\mathbf{M}. \tag{A.2}$$

ω is circular frequency, and n is the number of DOFs on each side of the segment. Matrices $\mathbf{K}$ and ω is circular frequency, and n is the number of DOFs on each side of the segment. Matrices $\mathbf{K}$ and The periodic conditions for the displacements and the equilibrium condition at the junction of two successive elements are are the stiffness and mass matrices of the segment as obtained from the FE model. Hysteretic damping can be introduced through complexity of the stiffness matrix. are the stiffness and mass matrices of the segment as obtained from the FE model. Hysteretic damping can be introduced through complexity of the stiffness matrix.

The dynamic stiffness matrix can be partitioned according to the left and right nodes of the segment so that Eq. (A.1) can be expressed as

$$\begin{bmatrix} \mathbf{D}_{LL} & \mathbf{D}_{LR} \\ \mathbf{D}_{RL} & \mathbf{D}_{RR} \end{bmatrix} \begin{Bmatrix} \boldsymbol{q}_L \\ \boldsymbol{q}_R \end{Bmatrix} = \begin{Bmatrix} \boldsymbol{f}_L \\ \boldsymbol{f}_R \end{Bmatrix}. \tag{A.3}$$

The subscripts L and R are designated for the left and right sides of the segment. Consider a series of segments of the waveguide as shown in Fig. 19. Continuity of displacement and force equilibrium of adjacent sections give

$$\begin{Bmatrix} \boldsymbol{q}_L^{N+1} \\ \\ \boldsymbol{f}_L^{N+1} \end{Bmatrix} = \begin{Bmatrix} \boldsymbol{q}_R^{N} \\ \\ -\boldsymbol{f}_R^{N} \end{Bmatrix}. \tag{A.4}$$

For each segment, the transfer matrix T can then be defined as

$$\mathbf{T} \begin{Bmatrix} \boldsymbol{q}_L^{N} \\ \\ \boldsymbol{f}_L^{N} \end{Bmatrix} = \begin{Bmatrix} \boldsymbol{q}_L^{N+1} \\ \\ \boldsymbol{f}_L^{N+1} \end{Bmatrix}. \tag{A.5}$$

The periodic conditions for the displacements and the equilibrium condition at the junction of two successive elements are $\boldsymbol{q}_R = \lambda\ \boldsymbol{q}_L$ and $\boldsymbol{f}_R =$ - $\lambda\ \boldsymbol{f}_L$ where the propagation constant $\boldsymbol{f}_L$ where the propagation constant

$$\lambda = e^{-ik\Delta}. \tag{A.6}$$

relates the right and left displacements and forces where k is the unknown wavenumber. Eq. (A.3) can be rearranged in the form of an eigenvalue problem (Duhamel *et al.*, 2006)

$$\mathbf{T} \begin{Bmatrix} \boldsymbol{q}_L \\ \\ \boldsymbol{f}_L \end{Bmatrix} = \lambda \begin{Bmatrix} \boldsymbol{q}_L \\ \\ \boldsymbol{f}_L \end{Bmatrix}. \tag{A.7}$$

The transfer matrix eigenvalue problem is solved at each frequency step to yield $2n$ solutions for the propagation constants and the corresponding wavenumbers as in Eq. (A.6). The wavenumber can be purely real, purely imaginary or complex, associated with a propagating, a nearfield (evanescent) or an oscillating decaying wave respectively.

(Zhong, 1995) has shown that that the eigenvalues of the transfer matrix occur in reciprocal pairs as λ_j^+ and $\lambda_j^- = 1/\ \lambda_j^+$. The corresponding wavenumbers are k_j^+ and $k_j^- =$ - k_j^+, representing the positive and negative going waves respectively. Furthermore, $\boldsymbol{\Phi}_j^+$ and $\boldsymbol{\Phi}_j^-$

are the associated right eigenvectors, where each wavemode is divided into displacement $\boldsymbol{q}$ and force $\boldsymbol{f}$ sub-vectors, i.e.

$$\boldsymbol{\Phi}_j = \begin{Bmatrix} \boldsymbol{\Phi}_q \\ \boldsymbol{\Phi}_f \end{Bmatrix}_j . \tag{A.8}$$

The positive-going waves are characterized by $\mid \lambda_j^+ \mid < 1$ and the negative going waves by $\mid \lambda_j^+ \mid > 1$. However, for $\mid \lambda_j^+ \mid = 1$, the associated waves are considered positive-going if they fulfil the condition $Re\left\{\boldsymbol{f_L^H}\dot{\boldsymbol{q}}_{\boldsymbol{L}}\right\} = Re\left\{i\omega\boldsymbol{f_L^H}\boldsymbol{q_L}\right\} < 0$ ¿ that determines the direction of powerflow. Evanescent waves contribute to the input response at discontinuities/boundaries but do not transfer energy (Mace, 1984).

Subsequently, the eigenvectors of the form of Eq. (A.8) are grouped into positive and negative going waves

$$\boldsymbol{\Phi}^+ = [\boldsymbol{\Phi}_1^+ \cdots \boldsymbol{\Phi}_n^+] \ ; \ \boldsymbol{\Phi}^- = [\boldsymbol{\Phi}_1^- \cdots \boldsymbol{\Phi}_n^-] \ ; \ \boldsymbol{\Phi} = [\boldsymbol{\Phi}^+ \quad \boldsymbol{\Phi}^-]. \tag{A.9}$$

The transformations between the physical domain, where the motion is described in terms of $\boldsymbol{q}$ and $\boldsymbol{f}$, and the wave domain, where the motion is described in terms of the wave amplitudes $\mathbf{a}^+$ and $\mathbf{a}^-$ travelling in the positive and negative directions respectively, are accomplished via

$$\begin{Bmatrix} \boldsymbol{q_L} \\ \boldsymbol{f_L} \end{Bmatrix} = \begin{bmatrix} \boldsymbol{\Phi}_q^+ & \boldsymbol{\Phi}_q^- \\ \boldsymbol{\Phi}_f^+ & \boldsymbol{\Phi}_f^- \end{bmatrix} \begin{Bmatrix} \mathbf{a}^+ \\ \mathbf{a}^- \end{Bmatrix}. \tag{A.10}$$

Rapidly decaying wave modes are removed due to their negligible contributions to the far field response, which can otherwise cause ill-conditioning problems. Thus, only m pairs of positive and negative going waves are retained based on a user-defined criterion. As a result, the size of the model will be smaller and the calculation time reduced.

ACI (**1995**). *Building code requirements for structural concrete: (ACI 318-95)* (Farmington Hills, MI : American Concrete Institute).

Amjad, U., Yadav, S., and Kundu, T. (**2015**). "Detection and quantification of diameter reduction due to corrosion in reinforcing steel bars," Structural Health Monitoring **14**, 532–543.

ANSYS (**2013**). ANSYS Mechanical APDL Element Reference .

Badiger, N., and Malipatil, K. (**2014**). "Parametric study on reinforced concrete beam using ANSYS," Civil and Environmental Research **6**, 88–94.

Duhamel, D., Mace, B. R., and Brennan, M. J. (**2003**). "Finite element analysis of the vibrations of waveguides and periodic structures," ISVR Technical Memorandum 922 .

Duhamel, D., Mace, B. R., and Brennan, M. J. (**2006**). "Finite element analysis of the vibrations of waveguides and periodic structures," Journal of Sound and Vibration **294**, 205–220.

El Masri, E. (**2018**). "Wave propagation in reinforced concrete beams with application to non-destructive testing," Ph.D. thesis, University of Southampton.

Ferguson, N., Halkyard, C., Mace, B., and Heron, K. (**2002**). "The estimation of wavenumbers in two-dimensional structures," Proceedings of the 2002 International Conference on Noise and Vibration Engineering, ISMA. 799–806.

Harland, N. R., Mace, B. R., and Jones, R. W. (**2001**). "Wave propagation, reflection and transmission in tunable fluid-filled beams," Journal of Sound and Vibration **241**, 735–754.

Houillon, L., Ichchou, M., and Jezequel, L. (**2005**). "Wave motion in thin-walled structures," Journal of Sound and Vibration **281**, 483–507.

Ichchou, M., Mencik, J., and Zhou, W. (**2009**). "Wave finite elements for low and mid-frequency description of coupled structures with damage," Computer Methods in Applied Mechanics and Engineering **198**, 1311–1326.

Jnaid, F., and Aboutaha, R. (**2015**). "Nonlinear finite element modeling of unboded steel reinforced concrete beams," International Journal of Civil, Environmental, Structural, Construction and Architectural Engineering **9**, 449–457.

Kharrat, M., Ichchou, M. N., Bareille, O., and Zhou, W. (**2014**). "Pipeline inspection using a torsional guided-waves inspection system. part 2: Defect sizing by the wave finite element method," International Journal of Applied Mechanics **06**, 1450035.

Kharrat, M., Zhou, W., Bareille, O., and Ichchou, M. N. (**2011**). "Identification and sizing of defects in pipelines by the wave finite element method using torsional guided waves," COMPDYN 2011, ECCOMAS Thematic Conference on Computational Methods in Structural Dynamics and Earthquake Engineering, Corfu, Greece .

Lee, S. K., Mace, B. R., and Brennan, M. J. (**2007**). "Wave propagation, reflection and transmission in non-uniform one-dimensional waveguides," Journal of Sound and Vibration

304, 31–49.

Li, R., and Zhang, Y. (**2011**). "Frequencies and modals analysis of prestressed concrete beam by ANSYS," Advanced Materials Research **243–249**, 769–773.

Mace, B. R. (**1984**). "Wave reflection and transmission in beams," Journal of Sound and Vibration **97**, 237–246.

Mace, B. R., Duhamel, D., Brennan, M. J., and Hinke, L. (**2005**). "Finite element prediction of wave motion in structural waveguides," Journal of the Acoustical Society of America **117**, 2835–2843.

Mencik, J. M., and Ichchou, M. N. (**2007**). "Wave finite elements in guided elastodynamics with internal fluid," International Journal of Solids and Structures **44**, 2148–2167.

Mitrou, G., Ferguson, N., and Rennou, J. (**2017**). "Wave transmission through two-dimensional structures by the hybrid fe/wfe approach," Journal of Sound and Vibration **389**, 484–501.

Renno, J., and Mace, B. R. (**2013**). "Calculation of reflection and transmission coefficients of joints using a hybrid finite element/wave and finite element approach," Journal of Sound and Vibration **332**, 2149–2164.

Saiidi, M., Douglas, B., and Feng, S. (**1994**). "Prestress force effect on vibration frequency of concrete bridges," Structural Engineering **120**, 2233–2241.

Waki, Y., Mace, B. R., and Brennan, M. J. (**2009**a). "Free and forced vibrations of a tyre using a wave/finite element approach," Journal of Sound and Vibration **323**, 737–756.

Waki, Y., Mace, B. R., and Brennan, M. J. (**2009**b). "Numerical issues concerning the wave and finite element method for free and forced vibrations of waveguides," Journal of Sound and Vibration **327**, 92–108.

Wang, F., Chan, T., Thambiratnam, D., and Tan, A. (**2010**). *Structural Health Monitoring: Vibration-Based Damage Detection and Condition Assesssment of Bridges* (IGI Global), Chap. 16, 230–243.

Yamakawa, J., and Murakami, H. (**1997**). "Longitudinal and flexural wave propagation in reinforced concrete columns," International Journal of Solids and Structures **34**, 4357–4376.

Zhong, W. X. (**1995**). "On the direct solution of wave propagation for repetitive structures," Journal of Sound and Vibration **181**, 485–501.

Zhou, W., and Ichchou, M. N. (**2010**a). "Wave propagation in mechanical waveguide with curved members using wave finite element solution," Computer Methods in Applied Mechanics and Engineering **199**, 2099–2109.

Zhou, W., and Ichchou, M. N. (**2010**b). "Wave scattering by local defect in structural waveguide through wave finite element method," Structural Health Monitoring **10**, 335–349.

Zima, B. (**2019**). "Guided wave propagation in detection of partial circumferential debonding in concrete structures," Sensors **19**, 2199.